COMMUNICATIONS IN SCIENCE AND TECHNOLOGY
Homepage: cst.kipmi.or.id

Microwave absorption performance of $La_{0.7}Sr_{0.3}MnO_3$/AC composite material based on activated carbon from *Gnetum gnemon* seed shell

Danang Pamungkas Priambodo[a], Sitti Ahmiatri Saptari[a,*], Arif Tjahjono[a], Maykel T. Manawan[b], Yana Taryana[c], Hadiyawarman[d], Ratna Isnanita Admi[e]

[a]*Department of Physics, Universitas Islam Negeri Syarif Hidayatullah Jakarta, Tangerang Selatan 15412, Indonesia*
[b]*Department of Propulsion Technology, Universitas Pertahanan, Bogor 16810, Indonesia*
[c]*Research Center for Telecommunication, National Research and Innovation Agency, Bandung 40135, Indonesia*
[d]*Research Center of Advanced Materials, National Research and Innovation Agency, Tangerang Selatan 15314, Indonesia*
[e]*Department of Physics, Universitas Indonesia, Depok 16424, Indonesia*

Article history:
Received: 28 May 2025 / Received in revised form: 11 August 2025 / Accepted: 21 October 2025

Abstract

The 5G internet network has been proven to facilitate daily life for people and render electronic devices such as smartphones as an integral component of people's daily routine. However, in conjunction with the ease of use, there is an issue of electromagnetic radiation. To cope with this issue, magnetic and dielectric composite microwave absorber materials have been undertaken. To address this, we investigated the limitations of activated carbon composite material from *Gnetum gnemon* seed shells (AC) on the microwave absorption ability of $(La_{0.7}Sr_{0.3}MnO_3)_{1-y}/(AC)_y$. The composite material $(La_{0.7}Sr_{0.3}MnO_3)_{1-y}/(AC)_y$ (y = 0; 0.3; 0.5; 0.7) was synthesized through a stirring process with a 96% ethanol catalyst using $La_{0.7}Sr_{0.3}MnO_3$ synthesized by sol-gel method and activated carbon material from *Gnetum gnemon* seed shell (AC) synthesized by chemical activation method. The XRD and SEM characterizations indicated a single-phase structure, with smaller crystals and particles that were uniformly distributed throughout the composite sample. The presence of activated carbon grains from *Gnetum gnemon* seed shells (AC) were observed between the $La_{0.7}Sr_{0.3}MnO_3$ grains in the composite sample. The EDS results confirmed the material's purity. VNA characterization demonstrated that $(La_{0.7}Sr_{0.3}MnO_3)_{1-y}/(AC)_y$ was capable of producing two reflection loss troughs with the largest absorption percentages recorded at 82.99% and 85.82% respectively within the frequency range of 8 – 12 GHz. This research highlights the significance of controlled composite composition in enhancing microwave absorption capability, particularly in perovskite-based composites with biomass-activated carbon, which holds a considerable promise for applications in electromagnetic wave attenuation and absorption technologies.

Keywords: Microwave absorber; composite; $La_{0.7}Sr_{0.3}MnO_3$/AC; biomass-based activated carbon; melinjo seed shell

1. Introduction

In In the era of the 5.0 industrial revolution, the Internet of Things has evolved to enter the 5th generation (5G) [1]. This has then resulted in the integration of electronic devices such as smartphones becoming an inseparable component of people's daily lives. However, this development has been shown to trigger electromagnetic wave pollution that has been demonstrated to have a negative impact, including electromagnetic radiation that can exert an effect on health. The phenomenon of electromagnetic radiation can cause hypersensitivity - a physiological disorder with neurological symptoms such as headaches, insomnia, excessive fatigue, and difficulty focusing. Other symptoms include restlessness accompanied by palpitations, nausea without any clear cause, muscle spasms, ringing in the ears, and depression [2–6]. To overcome electromagnetic radiation, Microwave Absorbing Material (MAM), a material that serves to reduce electromagnetic wave energy and convert it into heat energy, has been developed [7]. MAM exhibits permeability and permittivity values, as well as ideal characteristics such as strong absorption ability, thin thickness, light weight, and wide absorption bandwidth [4,5].

Perovskite-based materials are identified as one of the materials that possess the capability to absorb microwaves. The development of perovskite-based materials as MAM is conducted on manganate perovskite-based materials with the formula ABO_3. The doping of divalent ions on the A site has been demonstrated to result in high permittivity and permeability values in manganate perovskite-based materials, thereby resulting in ferromagnet or soft magnetic properties [8,9]. $La_{0.7}Sr_{0.3}MnO_3$ (LSMO) is a manganate perovskite-based material with ferromagnetic properties, rendering it suitable for

* Corresponding author.
Email: sitti.ahmiatri@uinjkt.ac.id
https://doi.org/10.21924/cst.10.2.2025.1727

use as a microwave absorbing material [10,11]. To enhance its absorption performance, LSMO is frequently prepared as a composite with other materials, such as graphite, which has good permittivity values and dielectric properties. This strategy has been proven effective in increasing the microwave absorption of LSMO [10].

Biomass is defined as a clean and renewable energy source derived from photosynthesized organic matter, including both products and residues [12]. Activated carbon materials obtained from biomass are increasingly utilized as MAMs because they are recyclable, environmentally friendly, and abundant in nature. To enhance its microwave absorption performance, it is possible to combine biomass activated carbon with ferromagnet material [4,13].

Melinjo (*Gnetum gnemon*) is an open-seeded plant native to Tropical Asia, Malenesia, and the Western Pacific [14]. As revealed in the horticultural production data from BPS (Central Bureau of Statistics) in 2021, Banten Province was the third largest Melinjo producer in Indonesia following Central Java and East Java. [15]. The large production of Melinjo in Banten has encouraged local people to process emping. However, the large-scale production of emping has led to a significant accumulation of melinjo seed shell waste that remains improperly managed, resulting in the accumulation of organic waste [15–19]. On the other hand, melinjo seed shell has been found to contain cellulose, hemicellulose, and lignin, suggesting its potential as a basic material to produce activated carbon [19]. Dwijayanti et al. [20] mentioned that *Gnetum gnemon* seed shell with a carbonization temperature of 400°C and 65% KOH as an activator has been shown to produce activated carbon with a surface area of 201.063 m^2/g.

Carbon has diverse types of allotropes, including colloidal carbon, carbon nanotubes, fullerenes carbon, graphite, graphene, colloidal sphere carbon, nanofiber carbon, porous carbon, nanowire carbon, and activated carbon [21]. The composition of different carbon allotropes with LSMO has been demonstrated their microwave absorption performance. Some of the composite materials are LSMO/CNT composites with 2 wt% CNT that exhibit a reflection loss value of -22.8 dB at 9.5 GHz [22], LSMO/RGO composite with 60% RGO demonstrating a reflection loss value of -31.81 dB in the range of 16 GHz - 18 GHz [23] and CF/LSMO composite with 50 wt% CF showing a reflection loss value of -17 dB at 9.4 GHz [24].

Activated carbon (AC) is one of the carbon allotropes that have not been composited with LSMO. It is particularly attractive as it can be efficiently synthesized from biomass, an abundant and sustainable resource. Biomass sources including banana peels and mango leaves are commonly employed as base materials in the production of activated carbon for microwave absorption. The utilization of banana peel activated carbon, in conjunction with KOH activator and carbonization temperature of 700°C for 1 hour, has been demonstrated to yield a reflection loss value of -40.62 dB at a frequency of 10.72 GHz [4]. The utilization of mango leaves, in conjunction with activated carbon and KOH activator produced a reflection loss value of -23.26 dB at 17.68 GHz. This process was conducted at carbonization temperature of 800°C for 2 hours [25].

Referring to the study by Dwijayanti et al., the activated carbon of the *Gnetum gnemon* seed shell has not been investigated as a microwave absorber [20]. In this study, the synthesis and characterization of $(La_{0.7}Sr_{0.3}MnO_3)_{1-y}/(AC)_y$ (y = 0; 0.3; 0.5; 0.7) composite material with activated carbon base material of *Gnetum gnemon* seed shell was conducted. Furthermore, the present study investigates the microwave absorption performance of a composite $La_{0.7}Sr_{0.3}MnO_3$ and activated carbon from *Gnetum gnemon* at X-band.

2. Materials and Methods

This section explains the synthesis of $(La_{0.7}Sr_{0.3}MnO_3)_{1-y}/(AC)_y$ composite material comprising a $La_{0.7}Sr_{0.3}MnO_3$ base material and *Gnetum gnemon* seed shell activated carbon. Furthermore, XRD, SEM-EDS, and VNA were employed in this study to characterize the composite and to determine its crystal structure, morphology, and microwave absorption performance.

2.1. Materials

The materials used included La_2O_3 (Merck 99.99%), $Sr(NO_3)_2$ (Merck 99%), $Mn(NO_3)_2.4H_2O$ (Merck 98.5%), $C_6H_8O_7.H_2O$ (Merck 99.5%), HNO_3 (Merck 65%), KOH (Sigma-Aldrich), NH_4OH (Merck 25%), ethanol 96%, aquadest and *Gnetum gnemon* seed shell waste.

2.2. $La_{0.7}Sr_{0.3}MnO_3$ synthesis

The synthesis of $La_{0.7}Sr_{0.3}MnO_3$ (LSMO) samples was conducted through the utilization of the sol-gel method. The synthesis started by weighing the precursors based upon stoichiometry, with $C_6H_8O_7.H_2O$ serving as the catalyst. The synthesis process was comprised of five stages: hydrolysis, gelatinization, dehydration, calcination, and sintering. The hydrolysis stage started by converting the La_2O_3 base from oxide to nitrate using HNO_3. Subsequently, all nitrate-based solutions from each precursor were mixed and stirred using a magnetic stirrer until homogeneous. The solution was stirred with a magnetic stirrer while being heated at 230ºC until the solution temperature reached ±70ºC. The gelatinization stage was initiated when the solution temperature reached ±70ºC, at which the solution was added with 25% NH_4OH until the pH of the solution became 7 (neutral) and a gel was formed. The gel was then heated on a hot plate at 90°C for 3 hours to evaporate the acid solvent. Furthermore, at the dehydration stage, the gel sample was reheated in an oven at 185ºC for approximately 3 hours. Afterwards, the sample (dry gel) was subjected to grinding and ground and the calcination stage was initiated using a furnace at 600°C for 6 hours for the decomposition of organic compounds in the sample. Following this, the sample was ground once more to enter the sintering stage using a furnace at 1000°C for 12 hours with a heating rate of 8°C/minute to strengthen the crystal bonds of the sample. The samples were then ground and sieved using a 200-mesh sieve to enter the composite and characterization stage.

2.3. Gnetum gnemon seed shell activated carbon synthesis

The synthesis of *Gnetum gnemon* seed shell activated carbon (AC) samples was conducted through the utilization of

chemical activation with 65% (w/v) KOH solution by referring to our previous research [26]. The seed shell waste of *Gnetum gnemon* was washed using distilled water prior to be dried. The carbonization of the *Gnetum gnemon* seed shell was conducted at a temperature of 400°C for 15 minutes. The carbonized sample was then activated with 65% (w/v) KOH at the ratio of 4:1 for 24 hours. Subsequently, the sample was stirred using a magnetic hot plate stirrer at 110 rpm at 110°C for 5 hours. The sample was then washed to neutral pH and dried at 110°C for 2 hours. It then went to the process of grinding for processing to the composite stage.

2.4. $La_{0.7}Sr_{0.3}MnO_3$/AC composite synthesis

The $(La_{0.7}Sr_{0.3}MnO_3)_{1-y}/(AC)_y$ composite sample was synthesized through a stirring process referring to the research of Al-Rabi et al [27]. In this study, LSMO samples were composited with *Gnetum gnemon* seed shell-activated carbon with a composition variation of y = 0; 0.3; 0.5; 0.7.

Table 1. Comparison of LSMO and AC sample composition for the synthesis of $(La_{0.7}Sr_{0.3}MnO_3)_{1-y}/(AC)_y$ composite material

Sample Code	Y Composition	$La_{0.7}Sr_{0.3}MnO_3$ (%)	*Gnetum gnemon* Seed Shell AC (%)
LSMO	0	100	-
LSMO/AC 30	0.3	70	30
LSMO/AC 50	0.5	50	50
LSMO/AC 70	0.7	30	70

The synthesis process started with the weighing of LSMO and AC samples in accordance to predetermined composition. Afterward, LSMO and AC samples were mixed with 96% ethanol being introduced as a catalyst. The solution homogenization process was carried out using a magnetic hot plate stirrer without heating (room temperature at 25ºC). Solution was stirred for 30 minutes and dehydrated via oven heating at a temperature of 85ºC for 1 hour prior to go to characterization process. The composition of $La_{0.7}Sr_{0.3}MnO_3$/AC composite sample is presented in Table 1.

2.5. Material characterization

Non-destructive tests were conducted to obtain information about the properties and characteristics of the material. At room temperature, the crystal structure of the samples was analyzed using X-Ray Diffraction (XRD) with a Cu-Ka radiation source (1.54056 Å) in the range of 3° - 90° with a step size of 0.02°. Scanning Electron Microscope and Energy Dispersive X-Ray Spectroscopy (SEM-EDS) with a maximum magnification of 30000× and an accelerating voltage of 20 kV were used to analyze the material morphology and elemental composition. The Vector Network Analyzer (VNA) was utilized to measure the absorption properties including reflection loss and through power in the X-band region in the range of 8-12 GHz with a step size of 0.2 GHz. The absorber material in this study was characterized as pure from each sample $(La_{0.7}Sr_{0.3}MnO_3)_{1-y}/(AC)_y$ (y = 0; 0.3; 0.5; 0.7), with a filling ratio of 100% for the test sample, and an absorber thickness of 1.5 mm.

3. Results and Discussion

This section discusses the results obtained from the characterization of the $(La_{0.7}Sr_{0.3}MnO_3)_{1-y}/(AC)_y$ (y = 0; 0.3; 0.5; 0.7) composite material, including crystal structure, morphology, and microwave absorption performance.

3.1. Crystal structure

In this study, the structural parameters resulting from the synthesis process of $La_{0.7}Sr_{0.3}MnO_3$ (LSMO) and $(La_{0.7}Sr_{0.3}MnO_3)_{0.5}/(AC)_{0.5}$ (LSMO/AC 50) samples were characterized using XRD. LSMO/AC 50 sample was selected for XRD characterization due to its balanced composition, which is a compromise between LSMO sample and AC sample.

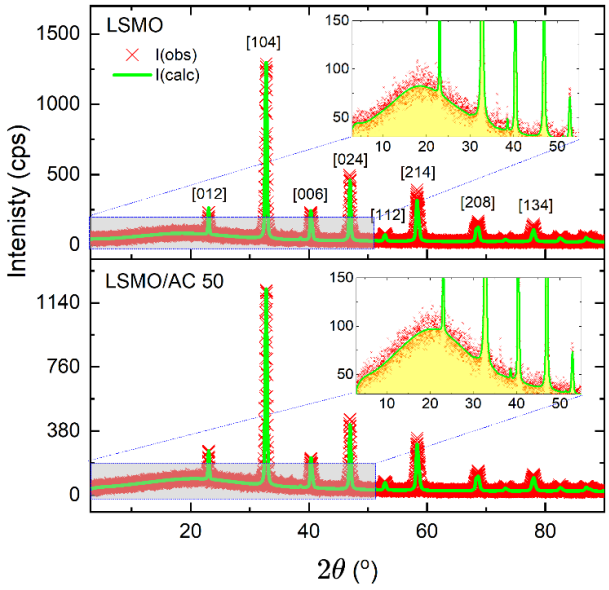

Fig. 1. XRD Pattern of LSMO and LSMO/AC 50. The cross red scatters indicate observation data and green line is Rietveld refinement result using GSAS-EXPGUI. Inset plots indicate amorphous background

Fig. 1 depicts a comparison of diffraction patterns of LSMO and LSMO/AC 50 samples. The diffraction pattern of the LSMO/AC 50 sample revealed the absence of activated carbon peaks. This phenomenon exhibits an inverse proportionality to the characteristics of composite materials, defined as materials consisting of two constituent materials or multiphase [28]. However, the diffraction pattern of the LSMO/AC 50 sample is in line with the findings of Wang et al. [29] and Guan et al. [30], stating that the absence of an activated carbon peak in composite sample is related to the amorphous characteristics of activated carbon. On the other hand, Ali et al. [31] mentioned that the diffraction pattern of amorphous material only shows a maximum average peak at a certain diffraction angle with low intensity in view of the absence of a periodic atomic arrangement.

The results of crystal structure characterization by XRD and qualitative analysis were conducted by Rietveld refinement method through GSAS-EXPGUI [32]. As demonstrated in Fig. 1, LSMO and LSMO/AC 50 samples exhibited a single phase with a goodness of fit (χ^2) of 1.000 and 1.002, respectively. The reference material for Rietveld refinement was the data from

$La_{0.7}Sr_{0.3}MnO_3$ [33] for LSMO and LSMO/AC 50 samples. The composite of AC into LSMO altered no crystal structure and space group of the material, however, it affected the value of lattice parameters of the material. From all three lattice parameters a, b, and c, the lattice c was the most affected with values of 13.367 Å and 13.365 Å for LSMO and LSMO/AC 50 samples, respectively. More complete information is presented in Table 2.

The crystal structure of LSMO remains unchanged when mixed with activated carbon, provided the mixing process is conducted through physical methods without applying high-temperature treatment [34], [35]. Consequently, the activated carbon composited into LSMO will appear in the XRD pattern as an amorphous phase. To evaluate this in the XRD data, we then employed the Degree of Crystallinity (DoC) equation [36]:

$$DoC = \frac{A_{peaks}}{A_{peaks} + A_{amorph}}, \quad (1)$$

where A represents the integral area under the curve of peak. As illustrated in Fig. 1, it is possible to differentiate between the crystalline peak area and the amorphous phase area, with the amorphous phase typically exhibiting extremely broad peaks. In this sample, the amorphous feature appeared in the range of 0–55° as evidenced by the magnified view of the angular region. Table 2 summarizes the calculation results, indicating an increase in the amorphous fraction of 16.9% after the addition of activated carbon into LSMO, confirming the successful incorporation of activated carbon into the composite.

Table 2. Crystal structure parameters of LSMO and LSMO/AC 50 samples

Parameter	LSMO	LSMO/AC 50
Space group	R - 3c (167)	
Crystal system	Rhombohedral	
a (Å)	5.496	5.495
b (Å)	5.496	5.495
c (Å)	13.367	13.365
Volume (Å^3)	349.672	349.582
Density (g/cm^3)	6.452	6.454
Crystallite size (nm)	21.601	18.562
Degree of Crystallinity		
Crystal (%)	62.85	46.95
Amorphous (%)	37.15	53.05
Discrepancy Factor		
wRp (%)	13.34	12.82
Rp (%)	10.29	9.98
χ^2	1.000	1.002
Mn-O Bond		
$\langle\theta_{Mn-O-Mn}\rangle$ (Å)	1.9523	1.9521
$\langle d_{Mn-O}\rangle$ (°)	166.4188	
Bandwidth (a.u)		
W (10^{-2})	9.5514	9.5543

The crystal size of the material obtained from the diffraction pattern. Specifically, the crystal sizes of the LSMO and LSMO/AC 50 samples were determined using the Debye-Scherrer method [37]:

$$D = \frac{k\lambda}{\beta \cos\theta}, \quad (2)$$

where D is the crystal size (nm), k is the Scherrer constant with a value of 0.9, λ is the X-ray wavelength (Cu-Kα, λ = 1.54056 Å), and β is the FWHM (rad). The crystal sizes of the LSMO and LSMO/AC 50 samples were 21.601 nm and 18.562 nm, respectively.

LSMO and LSMO/AC 50 samples exhibited Mn^{3+} and Mn^{4+} ions due to doping of Sr^{2+} ions into La^{3+} sites, thereby affecting the mobility of electrons in $(La_{0.7}Sr_{0.3}MnO_3)_{1-y}/(AC)_y$ material. This phenomenon is known as double exchange [38]. To determine the effect of double exchange on LSMO and LSMO/AC 50 samples, the bandwidth (W) value was calculated using Eq. (3) [39]:

$$W = \frac{\cos\left[\frac{1}{2}(\pi - \theta_{Mn-O-Mn})\right]}{d_{Mn-O}^{3.5}}, \quad (3)$$

where $\theta_{Mn-O-Mn}$ is the average angle formed from the nearest Mn-O-Mn atoms and d_{Mn-O} is the average distance from the nearest Mn and O atoms. A decline in the value of Mn-O bond length was identified in LSMO/AC 50 sample. This then resulted in an increase in bandwidth value in LSMO/AC 50 sample. The bandwidth of the material is related to strength of the double exchange interaction. A wider bandwidth can increase electron mobility between adjacent Mn ions. Otherwise, a reduced bandwidth can increase localization, thereby reducing the double exchange interaction [40].

3.2. Morphology

The geometric characteristics of a material, such as particle size, shape, internal structure, and surface topography, define its morphology. The shapes of crystal grains vary widely, including circular, angular, flake, beam, cube, rhombohedral, cylinder, flat, grain, spherical, ball, modular, dendritic, and needle [41]. The morphology of the samples was characterized by using a Scanning Electron Microscope (SEM) at a magnification of up to 30,000 times and an accelerating voltage of 20kV. The LSMO/AC 50 sample was selected as a representative composite sample for SEM-EDS characterization in view of its balanced composition between the LSMO sample and the AC sample. A composite material is defined as a material that consists of two constituent materials and does not react chemically but remains a physical unit in composite material [28]. This allows the morphology of LSMO and AC samples to coexist in the morphology of LSMO/AC 50 samples. Furthermore, the analysis of the SEM images was conducted with ImageJ software [42].

As illustrated in Fig. 2 (a) and (c), a comparative analysis of the morphology of LSMO and LSMO/AC 50 samples was conducted at a scale of 10 μm. The LSMO sample exhibited a hollow sharp coral-like morphology characterized with small spherical particles. Thanh et al. classified this structural characteristic as pseudo-spherical [11]. Fig. 3 refers to our

previous study [26], AC sample had a hollow plate-like morphological shape. This structural characteristic was termed "honeycomb-like structure" by Goel et al. [43] and "net-like structure" by Soleimani et al. [4]. As depicted in Fig. 2 (b) and (d) the mean particle sizes of LSMO and LSMO/AC 50 samples were 131.554 nm and 113.186 nm, respectively. A decrease in particle size in the samples was observed after the presence of composite at LSMO. This result is consistent with the decrease in crystal size as observed in the composite samples, as depicted in Table 2. The decrease in particle size was likely attributed to mechanical effects during the stirring process. The incorporation of activated carbon into LSMO promotes interparticle interactions under agitation, which may facilitate the breakdown of LSMO particle, which in turn led to smaller particle size. However, the particles were not classified as nanoscale since their average diameter exceeded 100 nm.

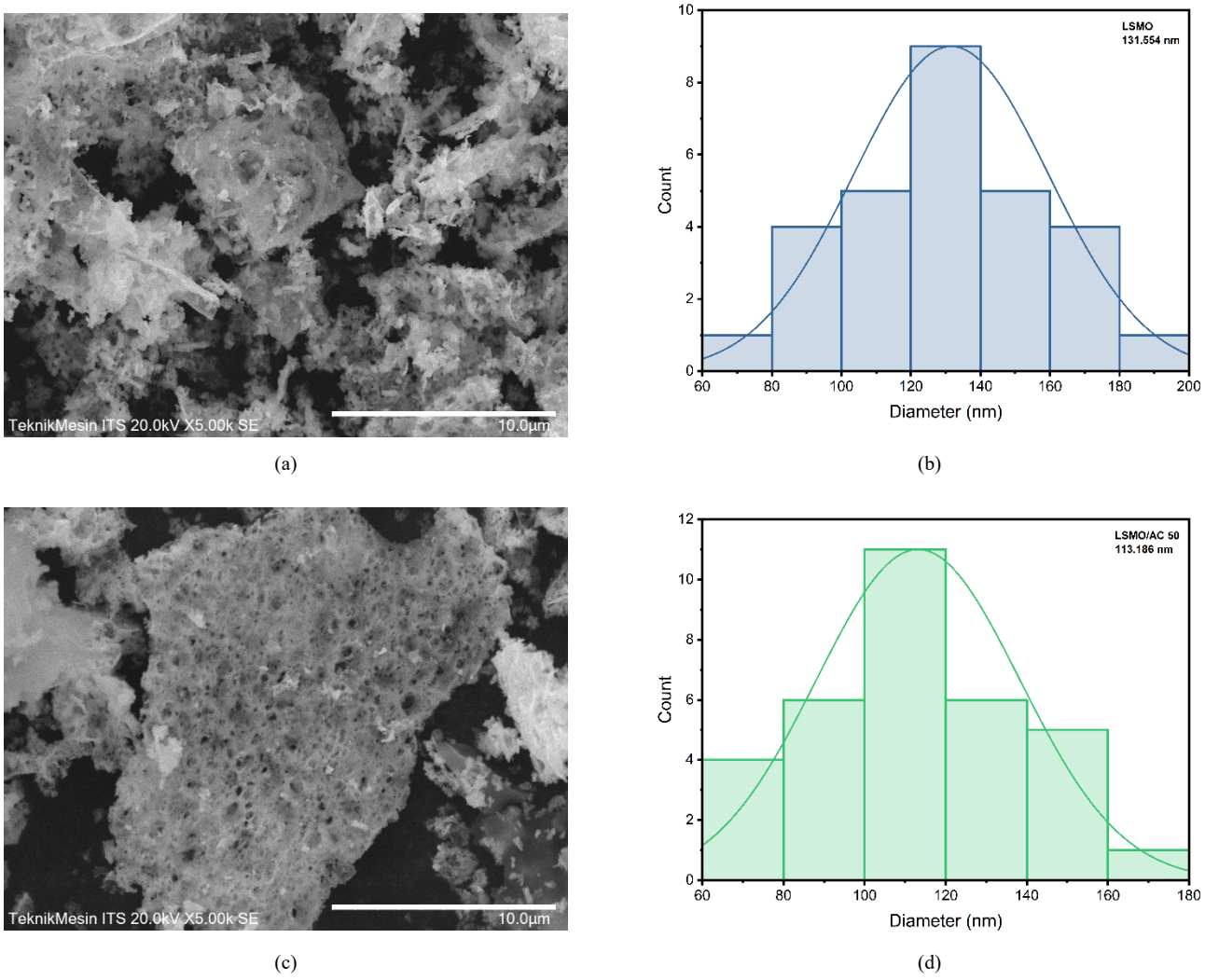

Fig. 2. Morphology and grain size of (a), (b) LSMO and (c), (d) LSMO/AC 50 samples

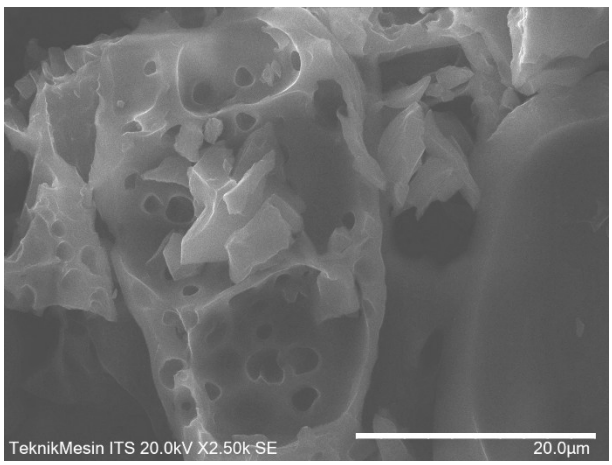

Fig. 3. Morphology of Gnetum gnemon seed shell activated carbon (AC) [26]

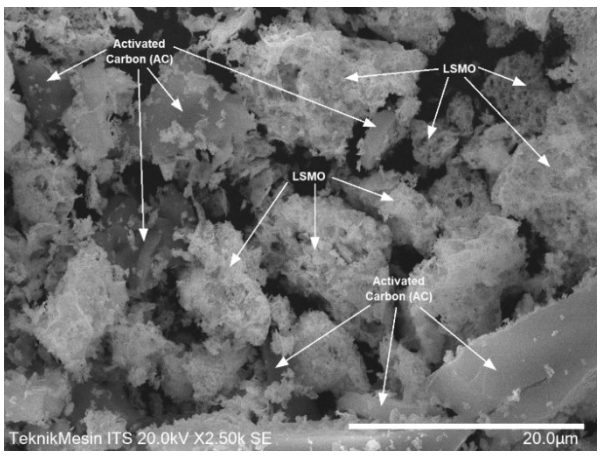

Fig. 4. Distribution of AC grains between LSMO grains in the LSMO/AC 50 sample

Fig. 4 presents the distribution of AC grains between LSMO grains in LSMO/AC 50 sample. LSMO/AC 50 sample exerted both morphological forms of LSMO and AC samples that coexisted with each other. The morphology is in accordance with the characteristics of composite materials, which is a material consisting of two constituent materials and does not react chemically, but remains a physical entity [28]. This finding indicates that AC has been composited into LSMO.

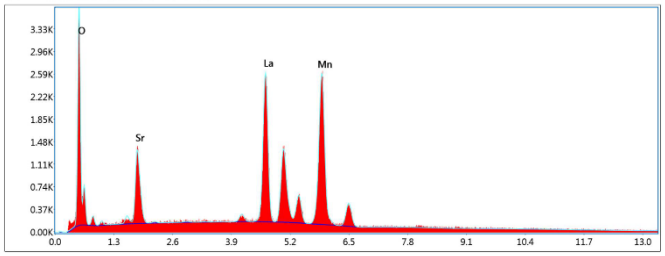

(a)

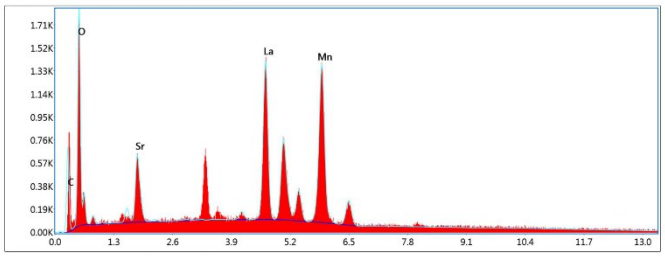

(b)

Fig. 5. EDS spectra of (a) LSMO and (b) LSMO/AC 50 samples

Table 3. Weight percent and particle size of LSMO and LSMO/AC 50 samples

Elements (wt%)	LSMO	LSMO/AC 50
La	41.85	35.68
Sr	10.36	7.02
Mn	27.29	22.67
O	20.50	20.88
C	-	13.75

Fig. 5 illustrates the EDS analysis of the LSMO and LSMO/AC 50 samples, revealing the absence of impurities. Only peaks corresponding to constituent elements appear, and the total weight percent (wt%) reaching 100% further validated this result. The appearance of carbon element in EDS spectrum of LSMO/AC 50 sample again indicated that AC has been composited into LSMO. Furthermore, Table 3 presents the weight percentages of the elemental composition of the LSMO and LSMO/AC 50 samples.

3.3. Microwave absorption performance

VNA instruments work based on scattering parameters. When electromagnetic waves of a specified frequency interact with the material under test, they are partially transmitted (output signal) and reflected (reflected signal), resulting in both reflected and transmitted signals. The quantification of reflected scattering, measured in decibels (dB), known as reflection loss (RL), indicates the absorption performance of the material against microwaves [44]. This can be calculated as:

$$RL\ (dB) = 20 \log \left| \frac{Z_{in}/Z_{out} - 1}{Z_{in}/Z_{out} + 1} \right|, \quad (4)$$

$$Z_{in}(\Omega) = Z_0 \sqrt{\frac{\mu_r}{\varepsilon_r}} \tan \mathrm{h} \left[j \left(\frac{2\pi f d}{c} \right) \sqrt{\mu_r \varepsilon_r} \right], \quad (5)$$

where Z_0 is the wave impedance of the free space with $Z_0 = \sqrt{\mu_0/\varepsilon_0}$, for this case $Z_{out} = Z_0$, f is input frequency (Hz), d is the sample thickness (mm), c is the speed of light (m/s), and j is the imaginary number. Meanwhile, μ_r (H/m) and ε_r (F/m) are relative permeability and permittivity, respectively, with definition $\mu_r = \mu' + j\mu''$ and $\varepsilon_r = \varepsilon' + j\varepsilon''$. Smaller reflected scattering value indicates that the performance of material is more excellent [39]. VNA testing provides data that explains the correlation between reflection loss and wave frequency.

In this study, LSMO samples were composited with AC into $(La_{0.7}Sr_{0.3}MnO_3)_{1-y}/(AC)_y$ (y = 0; 0.3; 0.5; 0.7). All samples were tested with VNA to evaluate the influence of AC composite composition on the microwave absorption performance of LSMO. Fig. 6 presents the comparison of the microwave absorption curves of $(La_{0.7}Sr_{0.3}MnO_3)_{1-y}/(AC)_y$ samples.

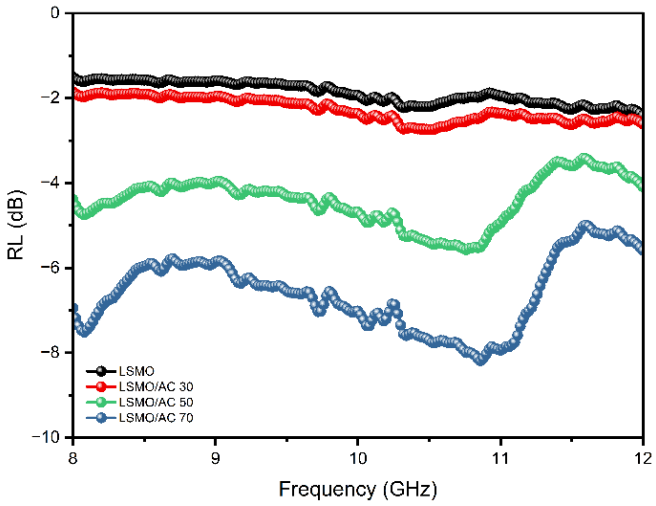

Fig. 6. Microwave absorption curve of LSMO, LSMO/AC 30, LSMO/AC 50, and LSMO/AC 70 samples

Table 4. Microwave absorption parameters of LSMO, LSMO/AC 30, LSMO/AC 50, and LSMO/AC 70 samples

Sample	Frequency (GHz)	Reflection Coefficient (Γ)	Reflection Loss (dB)	Through Power (%)
LSMO	10.30	0.765	-2.33	41.52
LSMO/AC 30	10.30	0.721	-2.84	47.98
LSMO/AC 50	8.08	0.571	-4.87	67.42
	10.86	0.518	-5.71	73.14
LSMO/AC 70	8.08	0.412	-7.69	82.99
	10.86	0.377	-8.48	85.82

The percentage of microwave absorption (through power) is obtained using Eq. (5) [45]:

$$Through\ power\ (\%) = 100(1 - \Gamma^2)\,, \qquad (6)$$

where Γ is the reflection coefficient ($\Gamma = 10^{RL/20}$). The $La_{0.7}Sr_{0.3}MnO_3$ (LSMO) sample has a single distinct reflection loss of -2.33 dB at a frequency of 10.30 GHz. The LSMO sample has a maximum absorption strength of 41.51%. The $(La_{0.7}Sr_{0.3}MnO_3)_{0.7}/(AC)_{0.3}$ (LSMO/AC 30) sample has one reflection loss distinct of -2.84 dB at 10.30 GHz. The LSMO/AC 30 sample has a maximum absorption strength of 47.98%. The $(La_{0.7}Sr_{0.3}MnO_3)_{0.5}/(AC)_{0.5}$ (LSMO/AC 50) sample has two reflection loss distinct of -4.87 dB and -5.71 dB at 8.08 GHz and 10.86 GHz, respectively. The LSMO/AC 50 sample has a maximum absorption strength of 73.14%. The $(La_{0.7}Sr_{0.3}MnO_3)_{0.7}/(AC)_{0.3}$ (LSMO/AC 70) sample has two reflection loss distinct of -7.69 dB and -8.48 dB at 8.08 GHz and 10.86 GHz, respectively. The LSMO/AC 70 sample has a maximum absorption strength of 85.82%. Table 4 presents the microwave absorption parameters for this material.

The effective absorption bandwidth (EAB) is defined as the free frequency range when the reflection loss value is less than -10 dB. The frequency range is effective because the material absorbs 90% of the incident electromagnetic waves under these conditions [46]. As demonstrated in Fig. 6, there was no EAB in all samples since reflection loss value was greater than -10 dB. This indicates that the samples absorb less than 90% of the microwaves. However, LSMO/AC 70 sample had the absorption values of 82.99% and 85.82% at frequencies of 8.08 GHz and 10.86 GHz, respectively, close to 90%. Thus, it can be stated that $(La_{0.7}Sr_{0.3}MnO_3)_{1-y}/(AC)_y$ composite sample still had good absorption ability.

These findings indicated that the material exhibited maximum microwave absorption capability in LSMO/AC 70 samples. This sample has been shown to produce two absorptions distinct at frequencies of 8.08 GHz and 10.86 GHz with percentage absorption of 82.99% and 85.82%, respectively. In microwave absorption theory, reflection loss is indicative of a material's capacity to absorb microwaves. High permittivity and permeability are critical to producing optimal reflection loss, with permeability affecting magnetic loss and permittivity affecting dielectric loss [39]. The $(La_{0.7}Sr_{0.3}MnO_3)_{1-y}/(AC)_y$ material is a combination of $La_{0.7}Sr_{0.3}MnO_3$ magnetic material and *Gnetum gnemon* seed shell activated carbon dielectric material. The permeability values of magnetic materials will affect magnetic loss. Meanwhile, dielectric materials possess a permittivity value that will affect dielectric loss. If the $(La_{0.7}Sr_{0.3}MnO_3)_{1-y}/(AC)_y$ material is exposed to microwaves, the *Gnetum gnemon* seed shell activated carbon material which acts as a dielectric material will absorb electric field contained in microwaves and cause a coulomb force. The charge will move with a certain acceleration to produce an electric current. This electric current causes heat, so it can be stated that the energy from microwaves is converted into heat energy. Conversely, the onset of electric current can also cause the generation of a magnetic field. The magnetic field arising due to dielectric material of *Gnetum gnemon* seed shell activated carbon will be strengthened by magnetic field originating from $La_{0.7}Sr_{0.3}MnO_3$ material. So, that two magnetic fields will mutually superpose destructively with magnetic field of incident microwave with same amplitude value but has a different phase [47].

The absorption ability of the material is closely related to its crystal and particle sizes. The XRD and SEM-EDS characterizations reveal a reduction in both parameters after compositing. This reduction increases the grain-specific surface area, thereby enhancing the reactivity of the samples through more frequent collisions. Consequently, the intrinsic resonance weakens the microwave energy, leading to higher microwave absorption [48]. This phenomenon demonstrates that incorporating AC into LSMO effectively improves its microwave absorption capability, consistent with Yan et al [10], who reported that carbon-based materials possess high permittivity and favorable dielectric properties that enhance microwave absorption.

Table 5. Comparison of absorption capabilities of the material in this work, LSMO/AC, with several references

Material	Composition	Thickness (mm)	Freq. (GHz)	Max. reflection loss (dB)	Ref.
LSMO/ *Gnetum gnemon* Seed Shell AC	70% AC	1.5	10.86	-8.48	This Work
CF/LSMO	50 wt% CF	3	9.4	-17.0	[24]
LSMO/ CNT	2 wt% CNT	3	9.5	-22.8	[22]
LSMO/ RGO	60% RGO	1.95	Range 16–18	-31.81	[23]
RGO/ LSMO	6.25 wt% RGO	2.5	10.7	-47.9	[10]

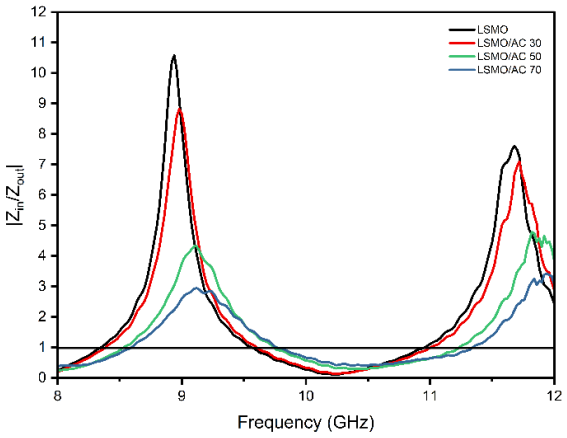

Fig. 7. Impedance ratio of LSMO, LSMO/AC 30, LSMO/AC 50, and LSMO/AC 70 samples

A comparison of microwave absorption capability of this paper with that of other papers that composite LSMO with other carbon allotropes can be seen in Table. 5. In comparison to the results of this paper, the highest absorption capability was shown by RGO/LSMO material (6.25 wt% RGO) in Ref. [10] with a reflection loss of -47.9 dB at 10.7 GHz. This occurred in relation to the thickness of tested sample that was very thick (2.5 mm) compared to the results of this paper (1.5 mm), where thickness is one of important factors that play a role in rising absorption in addition to composite composition as demonstrated in Eq. (5).

Table 6. Impedance matching of LSMO, LSMO/AC 30, LSMO/AC 50, and LSMO/AC 70 samples

Sample	Frequency (GHz)	$\lvert Z_{in}/Z_0 \rvert$	Z_{in}/Z_0 (%)
LSMO	10.30	0.1469	14.69
LSMO/AC 30	10.30	0.1625	16.25
LSMO/AC 50	8.08	0.2853	28.53
	10.86	0.5331	53.32
LSMO/AC 70	8.08	0.4161	41.62
	10.86	0.5821	58.22

Fig. 7 and Table 6 illustrate the impedance ratio and impedance matching of $(La_{0.7}Sr_{0.3}MnO_3)_{1-y}/(AC)_y$ samples, respectively. This indicates that the thickness of material also effects the impedance of sample match to reduced frequency. Impedance value (Z_0) used in this study referred to impedance instrument which is 50 Ω. The LSMO/AC 70 sample, which exerted the best absorption performance, demonstrated low match impedance values of 42.62% and 58.22% at 8.08 GHz and 10.86 GHz, respectively. This finding indicates a mismatch between thickness of tested material and reduced frequency. Percent impedance match can be considered high when it is close to 1 or equivalent to 100%, indicating that the thickness of tested material matches the reduced frequency range [25]. This mismatch also leads $(La_{0.7}Sr_{0.3}MnO_3)_{1-y}/(AC)_y$ sample not achieving an absorption strength above 90% at X-band frequencies with a thickness of 1.5 mm. So, re-engineering can be done by increasing thickness of the material to know the optimum thickness of $(La_{0.7}Sr_{0.3}MnO_3)_{1-y}/(AC)_y$ sample as a microwave absorber at X-band frequencies. In addition to increasing material thickness, testing can also be performed in frequency ranges other than X-band, such as S-band, C-band, or Ku-band to identify the optimum frequency of $(La_{0.7}Sr_{0.3}MnO_3)_{1-y}/(AC)_y$ material with a thickness of 1.5 mm.

4. Conclusion

The synthesis of $La_{0.7}Sr_{0.3}MnO_3$/AC composite material has been successfully achieved. $La_{0.7}Sr_{0.3}MnO_3$ (LSMO) has been synthesized through the sol-gel method, while activated carbon from *Gnetum gnemon* seed shell was synthesized through chemical activation method with 65% KOH activator. The LSMO/AC 50 sample was selected as a representative composite sample for XRD and SEM-EDS characterization because it exerted the similar composition of constituent materials. LSMO and LSMO/AC 50 samples had a single phase with a rhombohedral crystal system (R - 3c). No activated carbon peaks were found in the diffraction pattern of LSMO/AC 50 sample for activated carbon is amorphous. The LSMO sample had a hollow coral-like morphology with small spherical particles. In contrast, the LSMO/AC 50 sample exhibited both morphological forms of LSMO and AC sample. There was a decrease in particle size in samples following the composite process. The elemental composition of the LSMO and LSMO/AC 50 sample was confirmed by means of the EDS spectrum and mass weight measurements. As the composite composition increased, a decrease reflection loss value and increase absorption of the material were identified. The largest LSMO/AC 70 sample exhibited the most significant absorption strength with two distinct reflection loss at frequencies of 8.08 GHz and 10.86 GHz and absorption percentages of 82.99% and 85.82%, respectively. These findings provide further insight into perovskite-based and biomass activated carbon composite as potential microwave absorbers.

Acknowledgements

This work is funded by PUSLITPEN UIN Syarif Hidayatullah Jakarta research grant of UN.01/KPA/59/2024.

References

1. D. Sawitri, *Internet of Things Memasuki Era Society 5.0*, KITEKTRO: Jurnal Komputer, Informasi Teknologi, dan Elektro. 8 (2023) 31–35.
2. L. Cui, X. Han, F. Wang, H. Zhao, and Y. Du, *A review on recent advances in carbon-based dielectric system for microwave absorption*, Springer. 56 (2021) 10782–10811.
3. S. Zhang, Z. Jia, B. Cheng, Z. Zhao, F. Lu, and G. Wu, *Recent progress of perovskite oxides and their hybrids for electromagnetic wave absorption: a mini-review*, Adv Compos Hybrid Mater. 5 (2022) 2440–2460.
4. H. Soleimani, J. Y. Yusuf, H. Soleimani, L. K. Chuan, and M. Sabet, *Banana-Peel Derived Activated Carbon for Microwave Absorption at X-Band Frequency*, Synthesis and Sintering. 2 (2022) 120–124.
5. R. I. Admi, S. A. Saptari, A. Tjahjono, I. N. Rahman, and W. A. Adi, *Synthesis and characterization microwave absorber properties of La0.7(Ca1-xSrx)0.3MnO3 prepared by Sol-Gel method*, J Phys Conf Ser. 1816 (2021) 1–7.
6. R. A. Regia, R. A. Lestari, N. F. As'ad, and R. Zulkarnain, *Analisis Paparan Radiasi Elektromagnetik di Jaringan Distribusi 20 KV PT PLN (Persero) Unit Pelaksana Pelayanan Pelanggan (UP3) Payakumbuh*, Jurnal Ilmu Lingkungan. 21 (2023) 755–765.
7. L. Wang et al., *Recent progress of microwave absorption microspheres by magnetic-dielectric synergy*, Royal Society of Chemistry. 13 (2021) 2136–2156.
8. B. Nursanni, K. P. Putra, and G. Nastiti, *Sintesis dan Karakterisasi Penyerapan Gelombang Mikro pada Komposit PANi-Barium Heksaferrit Tersubstitusi Mn dan Ti-CFO*, Jurnal Pendidikan dan Teknologi Otomotif. 1 (2021) 1–7.
9. S. Sugiantoro, D. Wisnu, and A. Adi, *Karakterisasi Termal Bahan Magnetik Sistem La1-xBaxMnO3 (0<X<0,7) Sebagai Bahan Absorber Gelombang Elektromagnetik*, Prosiding Pertemuan Ilmiah Ilmu Pengetahuan dan Teknologi Bahan. (2012) 142–145.
10. K. Yan et al., *Broadband microwave absorber constructed by reduced graphene oxide/La0.7Sr0.3MnO3 composites*, RSC Adv. 9 (2019) 41817–41823.
11. T. D. Thanh et al., *Magnetic and microwave absorbing properties of La0.7Sr0.3MnO3 nanoparticles*, AIP Adv. 12 (2022) 035134.
12. E. Kurniawan, Z. Ginting, and R. Dewi, *Pemanfaatan Limbah Cangkang Biji Melinjo (Gnetum Gnemon) Sebagai Bahan Bakar Terbarukan dalam Pembuatan Biopelet*, Chemical Engineering Journal Storage. 2 (2022) 23–39.
13. E. Taer, L. Pratiwi, W. Sinta Mustika, and R. Taslim, *Three-dimensional pore structure of activated carbon monolithic derived from hierarchically bamboo stem for supercapacitor application*, Communications in Science and Technology. 5 (2020) 22–30.
14. E. S. Zulkarnain, *Inventarisasi dan Karakterisasi Melinjo (Gnetum Gnemon) Di Kota Solok*, Menara Ilmu. 15 (2021) 29–36.
15. Listiawati, N. Tri Yulvia, D. Permata Sari, N. Handayani, A. Faqih Robbani, and Y. Muluk, *Pemanfaatan Limbah Kulit Buah Melinjo*

(Gnetum Gnemon L) Menjadi Produk Olahan Keripik Kulit Buah Melinjo, Batara Wisnu Journal: Indonesian Journal of Community Services. 3 (2023) 540–548.

16. A. Mulyanto, E. Mawarsih, and R. Puspita Dewi, *Pengaruh Variasi Konsentrasi Perekat Terhadap Analisis Uji Nilai Kalor, Laju Pembakaran, Kadar Air, dan Kadar Abu Pada Briket Cangkang Biji Melinjo Sebagai Bahan Bakar Alternatif*, in Prosiding Seminar Nasional Riset Teknologi Terapan. (2023) 1–6.
17. S. F. Ayuningsih, N. Nurbaeti, and J. Gunawijaya, *Memorable Tourist Experience: Kunjungan Wisata ke Sentra Produksi Emping Melinjo Sebagai Daya Tarik Wisata Heritage*, Jurnal Hospitality dan Pariwisata. 9 (2023) 49–57.
18. T. Akbari, F. Panjaitan, and F. Dwirani, *Analisis Kelayakan Teknis dan Ekonomi Pengolahan Limbah Cangkang Melinjo (Gnetum gnemon) Sebagai Briket*, Jurnal Lingkungan dan Sumberdaya Alam (JURNALIS). 5 (2022) 132–146.
19. Slamet, Yuliusman, A. Dwijayanti, and S. Kartika, *Characteristics of Activated Carbon from Melinjo Shells Composed of TiO2 Nanoparticles*, Journal of Physics: Conference Series. 1477 (2020) 052012.
20. A. Dwijayanti, S. Kartika, and Yuliusman, *The effect of carbonization temperature and activator to the characteristics of melinjo shell (Gnetum genom) activated carbon*, AIP Conference Proceedings. 2175 (2019) 020057.
21. T. Rahman, M. A. Fadhlulloh, A. Bayu, D. Nandiyanto, and A. Mudzakir, *Review: Sintesis Karbon Nanopartikel*, Jurnal Integrasi Proses. 5 (2015) 120–131.
22. C. Y. Tsay, R. B. Yang, D. S. Hung, Y. H. Hung, Y. D. Yao, and C. K. Lin, *Investigation on electromagnetic and microwave absorbing properties of La0.7Sr0.3MnO3-δ/carbon nanotube composites*, J Appl Phys. 107 (2010) 09A502.
23. S. Dai, B. Quan, B. Zhang, X. Liang, and G. Ji, *Interfacial polarizations induced by incorporating traditional perovskites into reduced graphene oxide (RGO) for strong microwave response*, Dalton Transactions. 48 (2019) 2359–2366.
24. Y. Fang, H. Li, M. N. Akhtar, and L. Shi, *High-efficiency microwave absorber based on carbon Fiber@La0.7Sr0.3MnO@NiO composite for X-band applications*, Ceram Int. 47 (2021) 20438–20446.
25. P. Negi, A. K. Chhantyal, A. K. Dixit, S. Kumar, and A. Kumar, *Activated carbon derived from mango leaves as an enhanced microwave absorbing material*, Sustainable Materials and Technologies. 27 (2021) e00244.
26. M. Ishaq Nuras, S. Ahmiatri Saptari, A. Tjahjono, D. Pamungkas Priambodo, and A. Haiqal, *Synthesis and Characterization of Activated Carbon From Biomass Waste as A Microwave Absorber Material*, Al-Fiziya: Journal of Materials Science, Geophysics, Instrumentation and Theoretical Physics. 7 (2024) 12–32.
27. M. Al-Rabi, A. Tjahjono, and S. A. Saptari, *Analisis Fasa, Struktur Kristal dan Sifat Kemagnetan Material Komposit Berbasis Nd0,6Sr0,4MnO3/Fe2O3*, Al-Fiziya: Journal of Materials Science, Geophysics, Instrumentation and Theoretical Physics. 3 (2020) 114–122.
28. H. Ahmad et al., *Stealth technology: Methods and composite materials - A review*, Polym Compos. 40 (2019) 4457–4472.
29. H. Wang et al., *Biomass carbon derived from pine nut shells decorated with NiO nanoflakes for enhanced microwave absorption properties*, RSC Adv. 9 (2019) 9126–9135.
30. H. Guan et al., *Microwave absorption performance of Ni(OH)2 decorating biomass carbon composites from Jackfruit peel*, Appl Surf Sci. 447 (2018) 261–268.
31. A. Ali, Y. W. Chiang, and R. M. Santos, *X-Ray Diffraction Techniques for Mineral Characterization: A Review for Engineers of the Fundamentals, Applications, and Research Directions*, Minerals. 12 (2022) 205.
32. A. F. Gualtieri et al., *Quantitative phase analysis using the Rietveld method: Towards a procedure for checking the reliability and quality of the results*, Periodico di Mineralogia. 88 (2019) 147–151.
33. S. J. Hibble, S. P. Cooper, A. C. Hannon, I. D. Fawcett, and M. Greenblatt, *Local distortions in the colossal magnetoresistive manganates La0.70Ca0.30MnO3, La0.80Ca0.20MnO3 and La0.70Sr0.30MnO3 revealed by total neutron diffraction*, J. Phys.: Condens. Matter. (1999) 9221–9238.
34. R. Martínez, E. Cruz, S. Zografos, J. Soto, R. Palai, and C. Cabrera, *Integrating perovskite materials and bamboo-based activated carbon for electrochemical energy storage in hybrid supercapacitors*, J Energy Storage. 81 (2024) 110527.
35. A. R. Heiba, M. M. Omran, R. M. Abou Shahba, A. S. Dhmees, F. A. Taher, and E. El Sawy, *Compositing LaSrMnO3 perovskite and graphene oxide nanoribbons for highly stable asymmetric electrochemical supercapacitors*, Mater Sci Energy Technol. 8 (2025) 82–95.
36. M. Doumeng et al., *A comparative study of the crystallinity of polyetheretherketone by using density, DSC, XRD, and Raman spectroscopy techniques*, Polym Test. 93 (2021) 106878.
37. C. F. Holder and R. E. Schaak, *Tutorial on Powder X-ray Diffraction for Characterizing Nanoscale Materials*, American Chemical Society. 13 (2019) 7359−7365.
38. H. Li, *Synthesis of CMR manganites and ordering phenomena in complex transition metal oxides*, Jülich: Forschungszentrum Jülich. 4 (2008).
39. S. A. Saptari, J. Q. Syarifuddin, A. Tjahjono, H. Hadiyawarman, and G. E. Timuda, *Enhancement of microwave absorption ability of Nd0.67Sr0.33Mn1-xNix/2Tix/2O3 (x = 0, 0.03, and 0.06)*, Emergent Mater. 7 (2024) 2877–2890.
40. Z. J. Razi, S. A. Sebt, and A. Khajehnezhad, *Magnetoresistance temperature dependence of LSMO and LBMO perovskite manganites*, Journal of Theoretical and Applied Physics. 12 (2018) 243–248.
41. U. Ulusoy, *A Review of Particle Shape Effects on Material Properties for Various Engineering Applications: From Macro to Nanoscale*, MDPI. 13 (2023) 91.
42. C. T. Rueden et al., *ImageJ2: ImageJ for the next generation of scientific image data*, BMC Bioinformatics. 18 (2017) 529.
43. S. Goel, A. Garg, H. B. Baskey, M. K. Pandey, and S. Tyagi, *Studies on dielectric and magnetic properties of barium hexaferrite and bio-waste derived activated carbon composites for X-band microwave absorption*, J Alloys Compd. 875 (2021) 160028.
44. Y. Akinay, U. Gunes, B. Çolak, and T. Cetin, *Recent progress of electromagnetic wave absorbers: A systematic review and bibliometric approach*, ChemPhysMater. 2 (2023) 197–206.
45. F. A. Kurniawan, S. A. Saptari, A. Tjahjono, and D. S. Khaerudini, *Analysis Perovskite Material Absorber Based on Nd0.6Sr0.4MnxFe1/2(1-x)Ti1/2(1-x)O3 (x = 0, 0.1, 0.2) by Sol-Gel Method*, Journal of Physics: Theories and Applications. 6 (2022) 55.
46. X. Yang et al., *MOFs-Derived Three-Phase Microspheres: Morphology Preservation and Electromagnetic Wave Absorption*, Molecules. 27 (2022) 15.
47. K. Yusro and M. Zainuri, *Karakterisasi Material Penyerap Gelombang Radar Berbahan Dasar Karbon Aktif Kulit Singkong dan Barium M-Heksaferit*, Jurnal Sains dan Seni ITS. 4 (2015) 1–4.
48. Z. Qu et al., *Enhanced electromagnetic wave absorption properties of ultrathin MnO2 nanosheet-decorated spherical flower-shaped carbonyl iron powder*, Molecules. 27 (2022) 1.